Hydrol. Earth Syst. Sci. Discuss., 11, 5217–5250, 2014
www.hydrol-earth-syst-sci-discuss.net/11/5217/2014/
doi:10.5194/hessd-11-5217-2014

Hydrology and Earth System Sciences
Open Access
Discussions

A high resolution global scale groundwater model

I. E. M. de Graaf[1], **E. H. Sutanudjaja**[1], **L. P. H. van Beek**[1], **and M. F. P. Bierkens**[1,2]

[1]Department of Physical Geography, Faculty of Geosciences, Utrecht University, Utrecht, the Netherlands
[2]Unit Soil and Groundwater Systems, Deltares, Utrecht, the Netherlands

Received: 29 April 2014 – Accepted: 8 May 2014 – Published: 20 May 2014

Correspondence to: I. E. M. de Graaf (i.e.m.degraaf@uu.nl)

Published by Copernicus Publications on behalf of the European Geosciences Union.

Abstract

Groundwater is the world's largest accessible source of fresh water. It plays a vital role in satisfying needs for drinking water, agriculture and industrial activities. During times of drought groundwater sustains baseflow to rivers and wetlands, thereby supporting ecosystems. Most global scale hydrological models (GHMs) do not include a groundwater flow component, mainly due to lack of geohydrological data at the global scale. For the simulation of lateral flow and groundwater head dynamics a realistic physical representation of the groundwater system is needed, especially for GHMs that run at finer resolution. In this study we present a global scale groundwater model (run at 6′ as dynamic steady state) using MODFLOW to construct an equilibrium water table at its natural state as the result of long-term climatic forcing. The aquifer schematization and properties were based on available global datasets of lithology and transmissivities combined with estimated aquifer thickness of an upper unconfined aquifer. The model is forced with outputs from the land-surface model PCR-GLOBWB, specifically with net recharge and surface water levels. A sensitivity analysis, in which the model was run with various parameter settings, showed variation in saturated conductivity causes most of the groundwater level variations. Simulated groundwater heads were validated against reported piezometer observations. The validation showed that groundwater depths are reasonably well simulated for many regions of the world, especially for sediment basins ($R^2 = 0.95$). The simulated regional scale groundwater patterns and flowpaths confirm the relevance of taking lateral groundwater flow into account in GHMs. Flowpaths show inter-basin groundwater flow that can be a significant part of a basins water budget and helps to sustain river baseflow, explicitly during times of droughts. Also important aquifer systems are recharged by inter-basin groundwater flows that positively affect water availability.

HESSD
11, 5217–5250, 2014

1 Introduction

Groundwater is a crucial part of the global water cycle. It is the world's largest accessible source of fresh water and plays a vital role in satisfying basic needs of human society. It is a primary source for drinking water and supplies water for agriculture and industrial activities (Wada et al., 2014). During times of drought stored groundwater provides a buffer against water shortage and sustains baseflow to rivers and wetlands, thus supporting ecosystems and biodiversity. However, in many parts of the world groundwater is abstracted at rates that exceed groundwater recharge, causing groundwater levels to drop while baseflows to rivers are no longer sustained (Konikow, 2013; Gleeson et al., 2011).

Lateral groundwater flow and groundwater surface water interactions should be included in global scale hydrological models (GHMs) in order to understand how groundwater dynamics are affected by variations in recharge and human water use, especially as these GHMs progressively move towards finer resolutions (Wood et al., 2012). Several studies (e.g. Bierkens and van den Hurk, 2007; Fan et al., 2007) have suggested that lateral groundwater flows can be important for regional climate conditions as it influences soil moisture and thus the water cycle and energy exchanges within the lower atmosphere. Moreover, inter-basin groundwater flow can be a significant part of the water budget in a river basin under certain climate and geological conditions (Schaller and Fan, 2009). It helps to sustain river baseflows during times of droughts affecting ecosystems and wetlands and increasing surface water availability for human water use (de Graaf et al., 2014). Also large aquifer systems are additionally recharged by inter-basin groundwater flow, positively affecting water availability for groundwater abstraction.

Up to now, the current generation of GHMs typically does not include a lateral groundwater flow component mainly due to the lack of worldwide hydrogeological information. These data are available for parts of the developed world, but even there it is difficult to obtain data in a consistent manner. To cope with the unavailability of

HESSD
11, 5217–5250, 2014

hydrogeological data Sutanudjaja et al. (2011) proposed the use of global datasets of surface lithology and elevation for aquifer parameterization. This method was tested by building a groundwater flow model for the Rhine–Meuse basin (1 km resolution) with promising results. Similarly, Vergnes et al. (2012) used global and European datasets to delimit the main aquifer basins for France (at 0.5° resolution) and parameterized them on lithological information for France.

Recently, a pioneering study of Fan et al. (2013) presented a first ever high-resolution global groundwater table depth map. Their method however, does not include hydrogeological information (such as aquifer depths and transmissivities). Rather, it uses estimates from soil data and the river hydraulic connection between rivers and groundwater, which is the primary drainage for groundwater in humid regions, is ignored. Also, their model requires calibration to head observations.

In this paper we present a global scale groundwater model including an upper aquifer which is assumed to be unconfined. For the parameterization of the aquifer properties we relied entirely on available global lithological maps and databases (Gleeson et al., 2011; Hartmann and Moosdorf, 2012). To overcome the lack of information about aquifer thickness worldwide, it is estimated based on extrapolation of data available for the developed world, and can equally be extended to data-poor environments.

We forced the groundwater model with output from the global hydrological model PCR-GLOBWB (van Beek et al., 2011), specifically the net groundwater recharge and average surface water levels derived from routed channel discharge. This approach builds on earlier work by Sutanudjaja et al. (2011).

With this approach we are able to simulate groundwater heads of a first unconfined aquifer, providing a first-order estimate of the spatial variability of water table heads as a function of climate and geology. In this paper we limit ourselves to a steady-state simulation as a prelude to transient simulations in forthcoming work. Also we did not yet perform a formal calibration of the model. We performed a sensitivity analysis using a Monte Carlo framework in which we ran the model with various hydrogeological parameter settings. Simulated groundwater heads from all realizations were validated

HESSD
11, 5217–5250, 2014

against reported piezometer data worldwide and the parameter set with the highest coefficient of determination was used for further analysis. This resulted in a global map of average groundwater table depth in its natural state, i.e. in equilibrium with climate and without groundwater pumping. We simulated flowpaths to show the actual path through the subsoil that the groundwater follows from the location of infiltration towards the location of drainage. Flowpaths show areas where lateral groundwater flows are important and inter-basin groundwater flows are significant and contribute to water availability in neigbouring watersheds. It also gives an indication of travel time of groundwater following these flowpaths.

Here follows a description of the methods, in particular the parameterization of the upper aquifer, after which results of the sensitivity analysis and validation are presented. Next, the groundwater table depth map and flowpath maps for Europe and Africa are presented. We end with conclusions and discussion.

2 Methods

2.1 General

The hydrological model of the terrestrial part of the world (excluding Greenland and Antarctica) developed in this study consists of two parts; (1) the land surface model (PCR-GLOBWB) and (2) the steady state groundwater model (MODFLOW). Both the land-surface model and groundwater model are run at 6′ grid resolution (approximately 11 km at the equator). PCR-GLOBWB and MODFLOW are coupled offline where both models are run consecutively (Sutanudjaja et al., 2011).

2.1.1 Land surface model

The model PCR-GLOBWB is a global hydrological model that simulates hydrological processes in and between two soil stores (maximum depth 0.3 and 1.2 m respectively) and one underlying linear groundwater store. For a detailed description

HESSD
11, 5217–5250, 2014

of PCR-GLOBWB we refer to van Beek et al. (2011). In the original version of PCR-GLOBWB no lateral groundwater flow is simulated. Originally, groundwater flow within a cell is described as a linear store in PCR-GLOBWB and recharge is simulated as percolation to the groundwater store, minus capillary rise from the groundwater store to the soil. However, in the current MODFLOW model, the capillary rise is disabled to force a one-way coupling from PCR-GLOBWB to MODFLOW. We acknowledge this is a limitation in the current model approach.

We forced PCR-GLOBWB with 50 years (1960–2010) of meteorological data obtained from the ERA-40 reanalysis dataset (Uppala et al., 2005) for the period 1960–1999 extended with the ERA-interim reanalysis datasets (Dee et al., 2011) for the period 2000–2010 and bias-corrected it for monthly temperature, precipitation totals and numbers of wet days using CRU TS 2.1 monthly dataset (Mitchell and Jones, 2005) for the overlapping period (see de Graaf et al., 2014 for a more detailed description of this forcing dataset).

Before the actual simulation for the period 1960–2010 we spinned-up the model by running it back to back over the simulated period until a dynamic steady state was reached.

2.1.2 Groundwater model

In this study the linear groundwater store of PCR-GLOBWB is replaced by a MODFLOW groundwater layer (McDonald and Harbaugh, 2000; Schmitz et al., 2009), simulating lateral groundwater flows and groundwater heads of a single layer unconfined aquifer. Aquifer properties are prescribed and the MODFLOW layer is coupled via surface water levels and groundwater recharge to land surface model. Figure 1 illustrates the modelling strategy.

HESSD
11, 5217–5250, 2014

2.2 Estimating aquifer properties

Aquifer properties were initially based on two maps; (1) the high resolution global lithological map (GLiM) of Hartmann and Moosdorf (2012), and (2) the global permeability estimates of Gleeson et al. (2011).

The GliM describes 16 lithology classes (similar and expending on Dürr et al., 2005). We assumed that the lithological map represents the geology of the shallow subsurface accurately (Hartmann and Moosdorf, 2012). For the global permeability map the lithology classes of Dürr et al. (2005), that provide the basis for the lithological map of Hartmann and Moosdorf (2012), were paired to 5 combined hydrolithologies, defined as broad lithologic categories with similar hydrogeological characteristics (Gleeson et al., 2011) (see Table 1). They assumed that for all hydrolithologies there is no discernable dependence of permeability on scale, with the exception of carbonates, most likely due to karst. The resulting permeability map shows regional-scale permeability over the globe with the geometric mean permeability attributed to each hydrolithological unit. The geometric mean was obtained from calibrated permeabilities from groundwater models for units larger than 5 km in extent within 100 m depth.

Both maps are used to derive maps for storage capacities, recession coefficient, and saturated conductivities. The polygons in the GLiM, delieating a hydrological unit, are subsequently gridded to $30''$ (~ 1 km) and aggregated as the arithmetic and geometric mean respectively at the $6'$ resolution.

Because of the offline coupling and the lack of topographical detail in a $6'$ cell, the linear groundwater store is maintained, specifically for calculating baseflows above the drainage level to the surface water network using a cell-specific recession constant which accounts for aquifer properties and drainage density.

To calculate aquifer transmissivities (kD in $\mathrm{m\,d^{-1}}$), aquifer thicknesses are required. Since no globally consistent dataset on thickness is available, this is estimated using predominantly terrain attributes. Based on the assumption that unconfined productive aquifers coincide with sediment basins below river valleys the distinction is made

HESSD
11, 5217–5250, 2014

between (1) ranges with negligible sediment thickness, consisting mainly of hard rock with secondary permeability and (2) sediment basins with thick sediment layers.

Aquifer thickness was then estimated as follows:

1. Ranges and sediment basins were distinguished based on the difference between surface elevation and floodplain elevation. First, the floodplain elevations were mapped globally using the HydroSHEDS dataset at 30″ resolution and calculating the water levels belonging to bankfull discharges for each cell. The floodplain elevation of the lowest 30″ cell within a 6′ cell was taken as the floodplain elevation of the 6′ cell. Next, all cells with floodplain elevation within 50 m below the surface level were assumed to be part of the sediment basin underlain by an unconfined higher permeability sediment aquifer (Fig. 2, top panel). The defined sediment basins included 70 % of unconsolidated sediments mapped in the GLiM. The sediment basins consist of 56 % unconsolidated sediments, 25 % consolidated sediments and 19 % metamorphic or plutonic rocks. The latter is mainly found for the old cratons of Africa and the flat, recently glaciated areas of Laurasia.

2. For the sediment basins a measure expressing the relative difference between land surface elevation and floodplain elevation is calculated:

$$F'(x) = 1 - \frac{F(x) - F_{\min}}{F_{\max} - F_{\min}} \quad (1)$$

where $F(x)$ is the difference of surface and floodplain elevation at location x. $F_{\min}$ and $F_{\max}$ are the minimal and maximal difference, corresponding to a difference between land surface and floodplain elevation of 0 and 50 m respectively. This measure leads to a thinning layer further from the river towards the edge of the sediment basin. $F'(x)$ can be seen as the spatial frequency distribution of elevation above the floodplains. The associated z-score is calculated as:

$$Z(x) = G^{-1}(F'(x)) \quad (2)$$

HESSD
11, 5217–5250, 2014

where $G^{-1}()$ is the inverse of the standard normal distribution. Figure 3a shows a map of $Z(x)$.

3. Next, from available groundwater studies for the main aquifer systems of the USA (e.g. Central Valley California, Faunt et al., 2009, Mississippi basin, Clark and Hart, 2009) statistics of aquifer thickness of unconsolidated sediments were obtained. As a measure of difference between aquifer systems, for each study the average thickness was determined resulting in a range of average aquifer thickness of 50 to 500 m. Moreover, as a measure of thickness variation within aquifers systems, an average coefficient of variation (standard deviation divided by average) was determined from these studies. Because we assume aquifer thickness to be log-normally distributed (positively skewed) we determined the average thickness and coefficient of variation on the natural logarithms of thickness: $\overline{\ln D}$ and $C_{\overline{\ln D}}$ where $\overline{\ln D}$ is fixed and calculated from the average depth and standard deviation.

4. Accounting for the spatial uncertainty between and within aquifer systems the globally extrapolated thicknesses were assumed to follow a lognormal spatial frequency distribution for aquifer thickness with random parameters. Aquifer thickness was then calculated as:

$$\overline{\ln D} = U(\min; \max) \tag{3}$$

$$Y(x) = \overline{\ln D}(1 + Cv_{\overline{\ln D}} Z(x)) \tag{4}$$

$$D(x) = e^{Y(x)}. \tag{5}$$

This estimation was done in a Monte Carlo simulation of 100 runs, as the basis for the sensitivity analysis. The result of the best performing run (concluded after validation against observed groundwater heads) is presented in Fig. 3b.

HESSD
11, 5217–5250, 2014

After estimating the aquifer thicknesses transmissivities were calculated using the classic assumption that permeability decreases exponentially with depth (e.g. Beven and Kirkby, 1979; Ingebritsen and Manning, 1999) calculated as:

$$T(x) = \int_0^{D(x)} k_0 e^{\frac{-z}{\alpha}} \mathrm{d}z \quad (6)$$

where $T(x)$ is the transmissivity ($m^2\,d^{-1}$), k_0 ($m\,d^{-1}$) is conductivity close to the surface, as obtained from the hydrolitological map obtained from Hartmann and Moosdorf (2012) combined with the permeability values of Gleeson et al. (2011), z is depth and α is e-folding depth. The e-folding depth reflects the sediment-bedrock profile at a location, and depends strongly on terrain relief or slope (e.g. Summerfield and Hulton, 1994). α is determined by calibration by Miguez-Macho et al. (2008), and is adopted for this study. We assume that conductivities are horizontally homogeneous within a hydrolitological class. For mountain ranges low transmissivities are calculated. Note that therefore high permeable weathered regolith soils that develop on more gentle slopes of mountains are not accounted for and perched water tables that develop in these soils are not included in the model. Instead, the runoff associated with these perched water tables is taken care of in PCR-GLOBWB as stormflow or interflow from the second soil reservoir. A map of transmissivities (conductivity times depth) is given in Fig. 3c.

Note that our MODLFOW groundwater model is built at 6′ spatial resolution, which means that our MODLFOW cells are not rectangular, but have different length units and different cell areas. However, to account for the difference between actual cell length and width a spatially variable anisotropy factor can be introduced. We have not yet implemented this option, but will do so later.

HESSD
11, 5217–5250, 2014

2.3 Boundary conditions, recharge, and drainage levels

For large lakes and the ocean a Dirichlet boundary condition was assumed. For the ocean the groundwater head was set at 0 m, water levels of the lakes were based on the HydroSHEDS database.

The steady-state groundwater recharge, shown in Fig. 4 and obtained from PCR-GLOBWB, was used as input for the recharge package of MODFLOW. In the MODFLOW recharge package calculation, the input value of recharge is multiplied by the MODFLOW cell dimension to get a volume per unit time, $L^3 T^{-1}$. Because our MODFLOW cell dimension is 6′, the recharge input must be modified as follows:

$$RCH_{inp} = RCH_{act} \times \frac{A_{cell}}{A_{MF}} \quad (7)$$

where RCH_{inp} is the input for the recharge package in MODLFOW, RCH_{act} is actual input from the land surface model (both in md^{-1}) and A_{cell} and A_{MF} are "true" MODFLOW cell area and "apparent" MODFLOW cell area respectively. We used the MODFLOW river and drain package to incorporate interactions between groundwater bodies and the surface water network. The interactions are governed by actual groundwater heads and surface water levels. The latter can be obtained from the long-term average naturalized river discharge, $\overline{Q_{chn}}$, by using assumed channel properties: channel width, W_{chn} (L), channel depth, D_{chn} (L), Manning roughness coefficient, n ($L^2 T^{-1}$), and channel longitude slope, SI (–). Surface water levels were then used to simulate drainage levels.

The channel width is calculated using Lacey's formula (Lacey, 1930):

$$W_{chn} \approx P_{bkfl} = 4.8 \times Q_{bkfl}^{0.5} \quad (8)$$

where P_{bkfl} (m) is wetted perimeter, Q_{bkfl} is long-term averaged natural bankfull discharge ($m^3 d^{-1}$) and 4.8 ($s^{0.5} m^{-0.5}$) is a factor (Savenije, 2003). The bankflul discharge

HESSD
11, 5217–5250, 2014

is calculated from river discharges and occurs, as a role of thumb, every 1.5 year. In large natural braided rivers P_{bkfl} is slightly larger than W_{chn}. Combining Lacey's formula with Manning's formula (Manning, 1891) assuming a rectangular channel gives for channel depth:

$$D_{chn} = \left(\frac{n \times Q_{bkfl}^{0.5}}{4.8 \times SI^{0.5}} \right)^{\frac{3}{5}}. \quad (9)$$

By subtracting D_{chn} from surface elevation we estimated the bottom elevation of the river bed RBOT (m). The average river level can be translated from the long-term average naturalized river discharge $\overline{Q_{chn}}$ using the Manning formula:

$$\text{HRIV} = \text{RBOT} + \left(\frac{n \times \overline{Q_{chn}}}{B_{chn} \times SI^{0.5}} \right)^{\frac{3}{5}}. \quad (10)$$

The river bottom elevation and the river head are used as input for the river package in MODFLOW to calculate the flow between the river and aquifer: Q_{riv} ($m^3\,d^{-1}$). If the head in the cell connected to the river drops below the bottom of the river bed, water enters the groundwater system from the river at a constant rate. If the head is above the bottom of the river bed, water will either enter or leave the aquifer system depending on whether the head is above or below the head in the river. Q_{riv} is calculated as follows, where Q_{riv} is positive when water from the river enters the aquifer:

$$Q_{riv} = \begin{cases} c \times (\text{HRIV} - h) & \text{if } h > \text{RBOT} \\ c \times (\text{HRIV} - \text{RBOT}) & \text{if } h \leq \text{RBOT} \end{cases} \quad (11)$$

where h is groundwater head (m), and c is conductance ($m^2\,d^{-1}$) calculated as:

$$c = \frac{1}{\text{BRES}} \times P_{chn} \times L_{chn} \quad (12)$$

HESSD
11, 5217–5250, 2014

where BRES is bed resistance (d, taken 1 day here), L_{chn} (m) is the channel length (approximated the diagonal cell length as tortuosity here). The river package is used only for cells with $W_{chn} \geq 10$ m. To simulate smaller drainage elements the drain package is used. Water can only leave the groundwater system through the drain. The drainage Q_{drn} ($m^3\,d^{-1}$) is calculated as follows:

$$Q_{drn} = \begin{cases} c \times (\mathrm{DEM} - h) & \text{if } h > \mathrm{DEM} \\ c \times 0 & \text{if } h \leq \mathrm{DEM} \end{cases}. \quad (13)$$

The magnitude of Q_{riv} and Q_{drn}, which depends on the difference between groundwater head and surface water level, is the main component of the baseflow Q_{bf}, especially for flat sediment areas where groundwater flow is slow. However, this estimated baseflow is too small to satisfy the fast baseflow component originating from mountainous areas, where springs are tapping the groundwater. This fast baseflow component is included by assuming the groundwater above the floodplain is drained based on a linear reservoir component as follows:

$$Q_{bf} = -(Q_{riv} + Q_{drn}) + (JS_{3,flp}) \quad (14)$$

where $S_{3,flp}$ [m] is the groundwater storage above the floodplain and J (d^{-1}) is a recession coefficient parameterizated based on Kraaijenhof van der Leur (1958):

$$J = \frac{\pi(KD)}{4S_y L^2}. \quad (15)$$

Figure 4 shows the location of rivers and active drains.

2.4 Sensitivity analysis of aquifer properties and recharge

In groundwater modelling the transmissivity and groundwater recharge are important parameters and subject to large uncertainty. In this study we investigated the sensitivity

HESSD
11, 5217–5250, 2014

of the model outcome to changes in aquifer parameters, i.e. conductivity, thickness, and recharge.

For each parameter a Monte Carlo simulation of 100 samples were performed. This simulation followed a log normal distribution for layer thickness and saturated conductivity. For groundwater recharge a normal distribution was used. For layer thickness mean and standard deviation were obtained by combining several case studies of the USA and extrapolating this globally. Means and standard deviations of saturated conductivities per hydrolithological class were taken from Gleeson et al. (2011) (see Table 1). Mean and standard deviations for groundwater recharge were taken for the PCR-GLOBWB sensitivity study of Wada et al. (2014).

The variation in groundwater depth caused by changing one parameter was evaluated by calculating coefficients of variation, presented spatially. To obtain the uncertainty from the combination of these parameters, for each parameter 10 evenly distributed quantiles were combined into 1000 parameter sets to run the model with. Again variation in groundwater depth is evaluated by calculating coefficients of variation spatially.

2.5 Validation of groundwater depths

Simulated groundwater depths were validated against reported piezometer data (compiled dataset available from glowasis.eu). The average of the reported data was used if more than one observation was available in the 6′ grid cell, giving a total of 65 303 cells with observations worldwide. The water table head, instead of depth, was evaluated because the head measures potential energy that drives flow, and is therefore physically more meaningful. The coefficient of determination (R^2) and regression coefficient (α) were calculated for every run. Residuals, *res*, were calculated as *head simulated – head observed* and are presented spatially. Also relative residuals, *res rel*, calculated as *(head simulated-head observed)/heads observed* are presented spatially.

HESSD
11, 5217–5250, 2014

2.6 Simulating flowpaths

Particle tracking, using MODPATH (Pollock, 1994), was done to compute flowpaths and estimate travel times of groundwater flows. For this simulation cell-to-cell flux densities calculated by MODFLOW were used. A flowpath is computed by tracking the particle from one cell to the next until it reaches a boundary or sink. It shows the actual path through the subsoil that the groundwater follows from the location of infiltration towards the location of drainage. In our case the particle was stopped when it reached the ocean, a lake, or the local drainage (rivers or drains). It provides insights in regional scale groundwater movements and groundwater age, indicating areas where lateral groundwater flows are significant and inter-basin groundwater flows are important. The latter positivelly affect waterbudgets in neighbouring riverbasins or recharge to the aquifer system. Results are presented for Europe and Africa, showing paths and travel times.

3 Results and discussion

3.1 Sensitivity analysis

Figure 5 shows the coefficients of variation in simulated groundwater depths; Fig. 5a is the result of the 1000 runs with changing parameter settings for saturated conductivity, aquifer thickness, and recharge. In Fig. 5b–d, the result obtained by varying only one parameter is shown.

Figure 5a shows that the overall coefficient of variation is small. Higher coefficients of variation (CVs) are found for the Sahara and Australia desert, where recharge is low, transmissivities are high, and groundwater levels become disconnected from the surface. This emphasizes the influence of regional scale lateral flow. Higher variations are also found for areas with shallow groundwater tables and higher transmissivities and recharge, like the Amazone and Indus basin.

HESSD
11, 5217–5250, 2014

Figure 5b–d shows that saturated conductivity is the most important parameter controlling groundwater depths, as shown by the larger CVs. This is expected as the standard deviation of saturated conductivity is large for several hydrolitological classes (Table 1), changing saturated conductivity by orders of magnitude. A higher saturated conductivity leads to lower water tables and more significant regional groundwater flow, and vice versa.

The aquifer thickness does influence groundwater depth, but is of lower importance, than the effect of saturated conductivity. An increase of aquifer thickness leads to a greater transmissivity, but as the distribution of thickness is fixed ($F'(x)$ in Eq. 1), hence is the impact on calculated groundwater depths small.

Also the effect of recharge is small, a direct result of the small uncertainty in recharge that is included. Beside this, drainage is self-limiting; as recharge increases the water table rises and the hydraulic gradient is steepened, accelerating drainage and lowering the water table. This dampens the water table sensitivity to recharge uncertainties.

3.2 Validation of groundwater heads

Simulated groundwater depths (of the 1000 runs) validated against piezometer observations are shown in Fig. 6a. It should be noted that for most regions of the world no observation data are available or are incomplete (i.e. missing elevation measurement). While interpreting the validation results it should be noted that observations are biased towards river valleys, coastal ribbons, and the areas where large productive aquifers occur. Besides this, observations are taken at a certain moment in time, and thus are liable to seasonal effects and drawdown as a result of abstraction, while simulated groundwater depths are the steady state yearly average. Also, due the grid resolution small local valleys in the mountain ranges, resulting in higher local groundwater levels partly from infiltrating streams, are not captured. For the mountain ranges the deeper regional scale groundwater depth is simulated, while most likely the shallower groundwater from perched water tables formed in the soil layer overlying the basement rock is sampled. However, this process is included as storm flow in the land-surface model.

HESSD
11, 5217–5250, 2014

The coefficients of determination, R^2, are calculated for all runs and ranges between 0.75 and 0.87. For the 10 best performing runs R^2 ranges between 0.85 and 0.87. Given the fact that observations at higher and steeper terrains are most likely not sampling the simulated regional scale groundwater pattern but the more local, the R^2s are calculated again while excluding the possible perched water heads from the validation (i.e. considering observations in sediment basins only). The range of R^2s becomes than 0.90 to 0.95, and for the 10 best runs 0.945 and 0.946. (These are not the same 10 runs as before.)

Figure 6a gives the scatter plot of observed groundwater heads against simulated groundwater heads of the best performing overall run with in red the validation for observations in the sediment basins and in blue the observations on the ranges. Figure 6b shows the scatter plot the best performing run when considering observations in sediment basins only. Both runs show good model performance, especially for the sediment basins where shallow groundwater tables are simulated. The difference in model performance between the two runs for the ranges with deep groundwater tables is minimal.

In Fig. 7b the spatial distribution of residuals in groundwater depth for Europa and the USA is presented and the corresponding histograms are given in Fig. 7d. In addition, the distribution of observed groundwater head per residual class is indicated in colour in the histograms. Figure 7c shows the relative residual spatial distribution. Both histograms show a negative skew (longer tail to the left), this means that more negative residuals (underestimation of groundwater head) are calculated than positive, meaning more heads are underestimated than overestimated. The spatial distribution suggests that the negative bias tends to occur for higher and steeper terrains where deep groundwater tables are simulated, but where in reality shallower water tables occur in small sediment pockets in small valleys (e.g. slopes and piedmonts of the Rocky Mountains). It is partly due to the large scale of our model that it cannot capture these features. Residuals in lower flat areas where shallow groundwater tables are simulated are much smaller (e.g. Mississippi basin). The relative residuals are larger for areas

HESSD
11, 5217–5250, 2014

with shallow groundwater and smaller for the steeper terrains. The colored histograms show that mainly larger residuals are found when deeper groundwater tables are observed, and small residuals are found where shallow groundwater tables are observed.

3.3 Global groundwater depth map

Figure 8 shows the simulated steady-state (climate equilibrium) groundwater table depths at its natural state (without pumping), in meter below the land surface (result of the best performing run).

General patterns in water table depths can be identified. At the global scale, sea level is the main control of groundwater depths. Throughout the entire coastal ribbon shallow groundwater tables occur. These areas expand where flat coastal plains meet the sea, including major river basins like Mississippi, Indus and large wetlands. At the regional scale, recharge is the main control in combination with regional scale topography. For regions with high groundwater recharge rates shallow groundwater tables are simulated, for example the tropical swamps of the Amazone. The influence of the regional topography is also evident in the central Amazon and for the flat lowlands of South America as these regions receive water from the elevated areas.

Regions with low recharge rates correspond with deep groundwater where groundwater head gets disconnected from the local topography. The great deserts stand out (hyper-arid regions dotted in Fig. 8). Also for the mountain ranges of the world deep groundwater tables are simulated. As stated before, small local valleys causing higher local groundwater tables are not captured by the model due to the used grid resolution. The mountainous regions where perched water tables are likely to occur are masked in the figure with a transparent layer.

3.4 Groundwater flow paths and travel time

Figure 9 shows the simulated flowpaths for Europe and Africa where different colours indicate the simulated travel times. These figures show short and long inter-basin

HESSD
11, 5217–5250, 2014

flowpaths, that are stopped when they reach the local drainage, a lake, or the ocean. Long flowpaths are for example shown in East-Europe, where paths terminate submarine groundwater discharge. Also for Africa long flow paths are evident for the desert area. The flowpath simulations shows that especially for sediment areas, inter-basin groundwater flow is important and significant at least at longer time scales.

4 Conclusions

In this paper a global scale groundwater model of an upper unconfined aquifer layer is presented. A feasible and relative simple method is introduced to overcome the limited information available for aquifer parameterization; available global datasets for lithology and saturated conductivity were used such that the parameterization method can be expanded to data poor environments.

Applying this method we are able to produce a global picture of water table depths at fine resolution (6′) within acceptable accuracy in many part of the world, especially for sediment basins (R^2 = 0.95 and α = 0.84). The sediment basins are specific areas of interest, as these include the major aquifer systems of the world (e.g. Indus, Ganges, High Plains). For the higher and steeper terrain groundwater depths are in general overestimated compared to observations, likely because perched water tables, e.g. on hillsides, are not included in the groundwater model but are present in the observations. Additionaly, the model resolution and the aquifer property estimation are still too coarse to capture shallow water tables in small sediment pockets in small mountain valleys.

The results presented in this study confirm the relevance of taking lateral groundwater flow into account in global scale hydrological models. Short and long inter-basin flowpaths were simulated. The latter can be of major importance to sustain river baseflow in times of droughts supporting ecosystems and wetlands and increasing surface water availability for human water use. Or inter-basin groundwater flows can act as additional recharge to large aquifer systems, thus increasing water availability in these aquifers.

HESSD
11, 5217–5250, 2014

Obviously the model presented here must be considered as a first-order attempt towards global groundwater modelling and consequently has a number of limitations still that prevent it from simulating groundwater dynamics completely truthfully.

First of all, the model simulates a natural dynamic steady-state; it does not provide any information about groundwater fluctuations caused by climate (seasonal and annual) or human water use. Obviously, as we have estimated specific yield as well, extension to transient simulations is straight forward and will be attempted in a next study.

Secondly, only one unconfined layer is modeled here, while in reality, multi-layered aquifers including unconsolidated and consolidated layers can be present and groundwater be confined. Before we can include human groundwater use globally, these multilayered aquifers should be included in the model as this holds vital information on the accessibility and quality of global groundwater resources. However, the information on these aspects is sparse and incomplete.

Thirdly, capillary rise of the water table into the soil has not yet been implemented, although several studies have pointed out that it can affect soil moisture, evaporation, or even precipitation (e.g. Bierkens and van den Hurk, 2007; Fan et al., 2013; Lam et al., 2011). Further, there is no dynamic interaction between groundwater and surface water, as the drainage level of rivers does not change over time.

That being said, our model has the ability to capture the large scale distribution of groundwater levels and as such can serve as a starting point leading to a tool to assess groundwater level fluctuations and their sensitivity to human water intervention and climate.

The next step of this work will be to expand the current aquifer schematization with multi-layered and confined aquifer systems. The model will become transient and fully coupled to the land-surface model in order to incorporate capillary rise to the soil moisture and link river dynamics with groundwater. Human water use will be included as well. The goal will be to represent the impact of human water use on groundwater dynamics and river discharges. It will show where and when limits of groundwater

HESSD
11, 5217–5250, 2014

abstractions will be reached. This is vital information needed to ensure sustainable and efficient groundwater use, particularly for semi-arid regions where groundwater demand will intensify due to the increase of drought frequency and duration, combined with population growth, expansion of irrigation areas, and rising standard of living.

Acknowledgements. This study was funded by the Netherlands Organization for Scientific Research (NWO) in the project Planetary Boundaries Fresh Water Cycle.

References

Beven, K. J. and Kirkby, M. J.: Considerations in the development and validation of a simple physically based, variable contributing area model of catchment hydrology, in: Surface and subsurface hydrology, Proc. Fort Collins 3rd international hydrology symposium, July 1977, Fort Collins, 23–36, 1979. 5226

Bierkens, M. F. P. and van den Hurk, B. J. J. M.: Groundwater convergence as a possible mechanism for multi-year persistence in rainfall, Geophys. Res. Lett., 34, L02402, doi:10.1029/2006GL028396, 2007. 5219, 5236

Clark, B. and Hart, R.: The Mississippi Embayment Regional Aquifer Study (MERAS): Documentation of a groundwater-flow model contructed to assess water Availability in the Mississippi Embayment, Tech. Rep. 5172, US Geological Survey Scientific Investigations Report, US Geological Survey, Reston, Virginia, 2009. 5225

de Graaf, I. E. M., van Beek, L. P. H., Wada, Y., and Bierkens, M. F. P.: Dynamic attribution of global water demand to surface water and groundwater resources: effects of abstractions and return flows on river discharges, Adv. Water Resour., 64, 21–33, doi:10.1016/j.advwatres.2013.12.002, 2014. 5219, 5222

Dee, D., Uppala, S., Simmons, A., Berrisford, P., Poli, P., Kobayashi, S., Andrae, U., Balmaseda, M., Balsamo, G., Bauer, P., Bechtold, P., Beljaars, A., van de Berg, L., Bidlot, J., Bormann, N., Delsol, C., Dragani, R., Fuentes, M., Geer, A., Haimberger, L., Healy, S., Hersbach, H., Hólm, E., Isaksen, L., Kållberg, P., Köhler, M., Matricardi, M., Mcnally, A., Monge-Sanz, B., Morcrette, J.-J., Park, B.-K., Peubey, C., de Rosnay, P., Tavolato, C., Thépaut, J.-N., and Vitart, F.: The ERA-Interim reanalysis: configuration and performance of the data assimilation system, Q. J. Roy. Meteorol. Soc., 137, 553–597, 2011. 5222

HESSD
11, 5217–5250, 2014

Dürr, H. H., Meybeck, M., and Dürr, S. H.: Lithologic composition of the Earth's continental surfaces derived from a new digital map emphasizing riverine material transfer, Global Biogeochem. Cy., 19, GB4S10, doi:10.1029/2005GB002515, 2005. 5223
Fan, Y., Miguez-Macho, G., Weaver, C. P., Walko, R., and Robock, A.: Incorporating water table dynamics in climate modeling: 1. Water table observations and equilibrium water table simulations, J. Geophys. Res.-Atmos., 112, D10125, doi:10.1029/2006JD008111, 2007. 5219
Fan, Y., Li, H., and Miguez-Macho, G.: Global patterns of groundwar table depth, Science, 339, 940–943, doi:10.1126/science.1229881, 2013. 5220, 5236
Faunt, C. C. (Ed.): Groundwater availability of the Central Valley Aquifer, US Geological Survey Professional Paper 1766, US Geological Survey, California, p. 255, 2009. 5225
Gleeson, T., Smith, L., Moosdorf, N., Hartmann, J., Dürr, H. H., Manning, A. H., van Beek, L. P. H., and Jellinek, A. M.: Mapping permeability over the surface of the Earth, Geophys. Res. Lett., 38, L02401, doi:10.1029/2010GL045565, 2011. 5219, 5220, 5223, 5226, 5230, 5241
Hartmann, J. and Moosdorf, N.: The new global lithological map database GLiM: a representation of rock properties at the Earth surface, Geochem. Geophy. Geosy., 13, Q12004, doi:10.1029/2012GC004370, 2012. 5220, 5223, 5226, 5241
Ingebritsen, S. and Manning, C.: Geological implications of a permeability-depth curve for the continental crust, Geology, 27, 1107–1110, doi:10.1130/0091-7613(1999)027<1107:GIOAPD>2.3.CO;2, 1999. 5226
Konikow, L. F.: Overestimated water storage, Nat. Geosci., doi:10.1038/ngeo1659, in press, 2013. 5219
Kraaijenhof van der Leur, D.: A study of non-steady grounground flow with special reference to a reservoir coefficient, de ingenieur, 70, 87–94, 1958. 5229
Lacey, G.: Stable cchannel in alluvium, P. I. Civ. Eng., 229, 259–292, 1930. 5227
Lam, A., Karssenberg, D., van den Hurk, B. J. J. M., and Bierkens, M. F. P.: Spatial and temporal connections in groundwater contribution to evaporation, Hydrol. Earth Syst. Sci., 15, 2621–2630, doi:10.5194/hess-15-2621-2011, 2011. 5236
Manning, R.: On the flow of water in open cchannel and pipes, Transactions of Institution of Civil Engineers of Ireland, Dublin, 161–207, 1891. 5228
McDonald, M. G. and Harbaugh, A. W.: MODFLOW-2000, the US Geological Survey modular ground-water model – User guide to modularmodular concepts and the Ground-Water Flow Process, Tech. rep., US Geological Survey, Reston, Virginia, 2000. 5222

HESSD
11, 5217–5250, 2014

Miguez-Macho, G., Li, H., and Fan, Y.: Simulated water table and soil moisture climatology over north america, B. Am. Meteorol. Soc., 89, 663–672, doi:10.1175/BAMS-89-5-663, 2008. 5226

Mitchell, T. D. and Jones, P. D.: An improved method of constructing a database of monthly climate observations and associated high-resolution grids, Int. J. Climatol., 25, 693–712, doi:10.1002/joc.1181, 2005. 5222

Pollock, D.: User's Guide for MODPATH/MODPATH-PLOT, version 3: A particle tracking post-processing package for MODFLOW, the US Geological Survey finite-difference groundwater flow model, Tech. rep., US Geological Survey Open-File Report 94-464, US Geological Survey, Reston, Virginia, 1994. 5231

Savenije, H. H.: The width of a bankfull channel; Lacey's formula explained, J. Hydrol., 276, 176–183, doi:10.1016/S0022-1694(03)00069-6, 2003. 5227

Schaller, M. F. and Fan, Y.: River basins as groundwater exporters and importers: implications for water cycle and climate modeling, J. Geophys. Res.-Atmos., 114, D04103, doi:10.1029/2008JD010636, 2009. 5219

Schmitz, O., Karssenberg, D., van Deursen, W., and Wesseling, C.: Linking external components to spatio-temporal modeling framework: coupling MODLFW and PCRaster, Environ. Modell. Softw., 24, 1088–1099, doi:10.1016/j.envsoft.2009.02.018, 2009. 5222

Summerfield, M. and Hulton, N.: Natural controls of fluvial denudation rates in major world drainage basins, J. Geophys. Res., 99, 13871–13883, 1994. 5226

Sutanudjaja, E. H., van Beek, L. P. H., de Jong, S. M., van Geer, F. C., and Bierkens, M. F. P.: Large-scale groundwater modeling using global datasets: a test case for the Rhine-Meuse basin, Hydrol. Earth Syst. Sci., 15, 2913–2935, doi:10.5194/hess-15-2913-2011, 2011. 5220, 5221, 5242

Uppala, S. M., Kållberg, P. W., Simmons, A. J., Andrae, U., Bechtold, V. D. C., Fiorino, M., Gibson, J. K., Haseler, J., Hernandez, A., Kelly, G. A., Li, X., Onogi, K., Saarinen, S., Sokka, N., Allan, R. P., Andersson, E., Arpe, K., Balmaseda, M. A., Beljaars, A. C. M., Berg, L. V. D., Bidlot, J., Bormann, N., Caires, S., Chevallier, F., Dethof, A., Dragosavac, M., Fisher, M., Fuentes, M., Hagemann, S., Hólm, E., Hoskins, B. J., Isaksen, L., Janssen, P. A. E. M., Jenne, R., Mcnally, A. P., Mahfouf, J.-F., Morcrette, J.-J., Rayner, N. A., Saunders, R. W., Simon, P., Sterl, A., Trenberth, K. E., Untch, A., Vasiljevic, D., Viterbo, P., and Woollen, J.: The ERA-40 re-analysis, Q. J. Roy. Meteorol. Soc., 131, 2961–3012, doi:10.1256/qj.04.176, 2005. 5222

HESSD
11, 5217–5250, 2014

van Beek, L. P. H., Wada, Y., and Bierkens, M. F. P.: Global monthly water stress: 1. Water balance and water availability, Water Resour. Res., 47, W07517, doi:10.1029/2010WR009791, 2011. 5220, 5222

Vergnes, J.-P., Decharme, B., Alkama, R., Martin, E., Habets, F., and Douville, H.: A simple groundwater scheme for hydrological and climate applications: description and offline evaluation over france, J. Hydrometeorol., 13, 1149–1171, doi:10.1175/JHM-D-11-0149.1, 2012. 5220

Wada, Y., Wisser, D., and Bierkens, M. F. P.: Global modeling of withdrawal, allocation and consumptive use of surface water and groundwater resources, Earth Syst. Dynam., 5, 15–40, doi:10.5194/esd-5-15-2014, 2014. 5219, 5230

Wood, E. F., Roundy, J. K., Troy, T. J., van Beek, R., Bierkens, M., Blyth, E., de Roo, A., Döll, P., Ek, M., Famiglietti, J., Gochis, D., van de Giesen, N., Houser, P., Jaffe, P., Kollet, S., Lehner, B., Lettenmaier, D. P., Peters-Lidard, C. D., Sivapalan, M., Sheffield, J., Wade, A. J., and Whitehead, P.: Reply to comment by Keith, J. Beven and Hannah, L. Cloke on "Hyperresolution global land surface modeling: Meeting a grand challenge for monitoring Earth's terrestrial water", Water Resour. Res., 48, W01802, doi:10.1029/2011WR011202, 2012. 5219

HESSD
11, 5217–5250, 2014

Table 1. Lithologic and hydrolihologic categories.

Lithilogy classes[a]	Hydrolithology classes[b]	log k μ_{geo} [m^2][b]	σ [m^2][b]
Unconsolidated sediments	unconsolidated	−13.0	2.0
	c.g. unconsolidated	−10.9	1.2
	f.g. unconsolidated	−14.0	1.8
Siliciclastic sediments	siliciclastic sedimentary	−15.2	2.5
	c.g. siliciclastic sedimentary	−12.5	0.9
	f.g. siliciclastic sedimentary	−16.5	1.7
Mixed sedimentary rocks Carbonate sedimentary rocks Evaporites	Carbonate	−11.8	1.5
Acid volcanic rocks Intermediate volcanic rocks Basic volcanic rocks	Crystalline	−14.1	1.5
Acid plutonic rocks Intermediate plutonic rocks Basic plutonc rocks pyroclastics metamorphic	Volcanic	−12.5	1.8
water bodies Ice and Glaciers	not assigned	–	–

[a] Hartmann and Moosdorf (2012).
[b] Based on Gleeson et al. (2011), log k μ_{geo} is the geometric mean logarithmic permeability; σ is the standard deviation; f.g. and c.g. are fine-grained and coarse-grained, respectivaly.

HESSD
11, 5217–5250, 2014

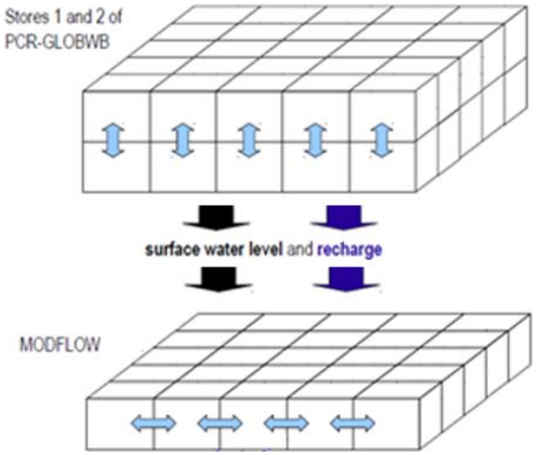

Figure 1. Model structure used to couple the land-surface model PCR-GLOBWB with the groundwater model MODFLOW: first average annual net recharge and average annual channel discharge is calculated with PCR-GLOBWB. THe latter is translated into surface water levels. Both recharge and surface water levels are used to force MODFLOW (after Sutanudjaja et al., 2011).

HESSD
11, 5217–5250, 2014

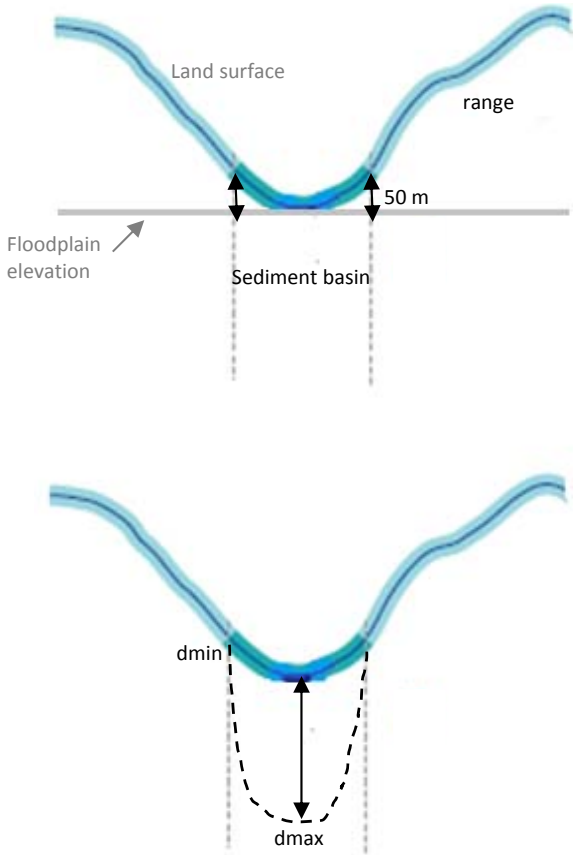

Figure 2. Top panel: definition of sediment basins and ranges, based on terrain attributes (land surface elevation and floodplain elevation). Bottom panel: estimation of aquifer thickness.

HESSD
11, 5217–5250, 2014

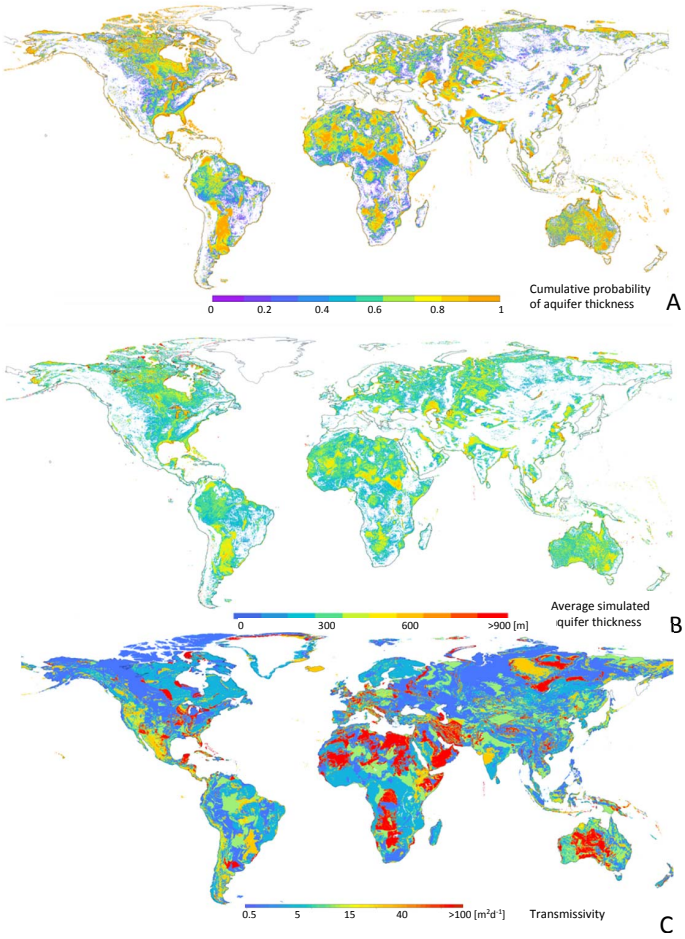

Figure 3. Calculated cumulative probability of aquifer thickness, calculated aquifer thickness, and calculated tranmissivities.

HESSD
11, 5217–5250, 2014

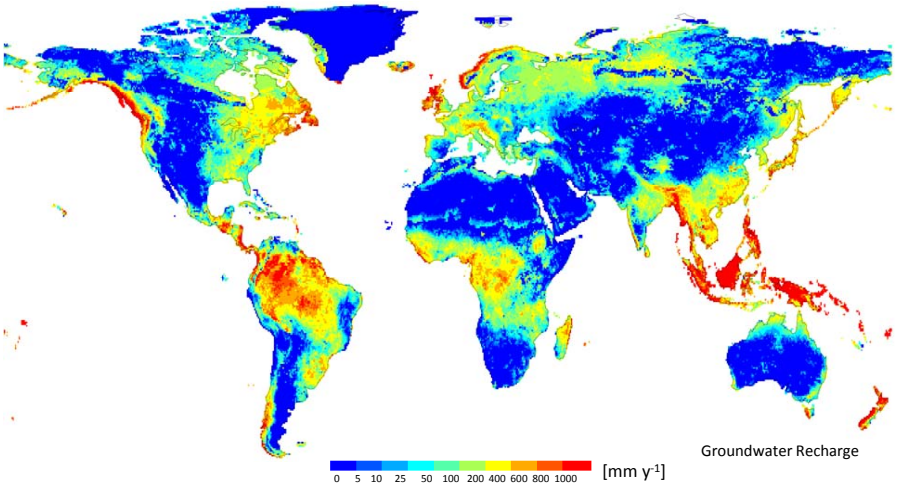

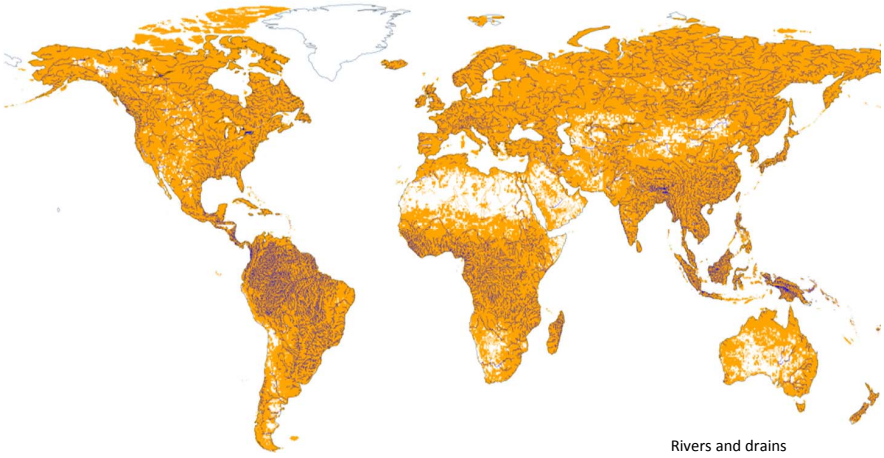

Figure 4. Locations of rivers and drains and groundwater recharge input.

HESSD
11, 5217–5250, 2014

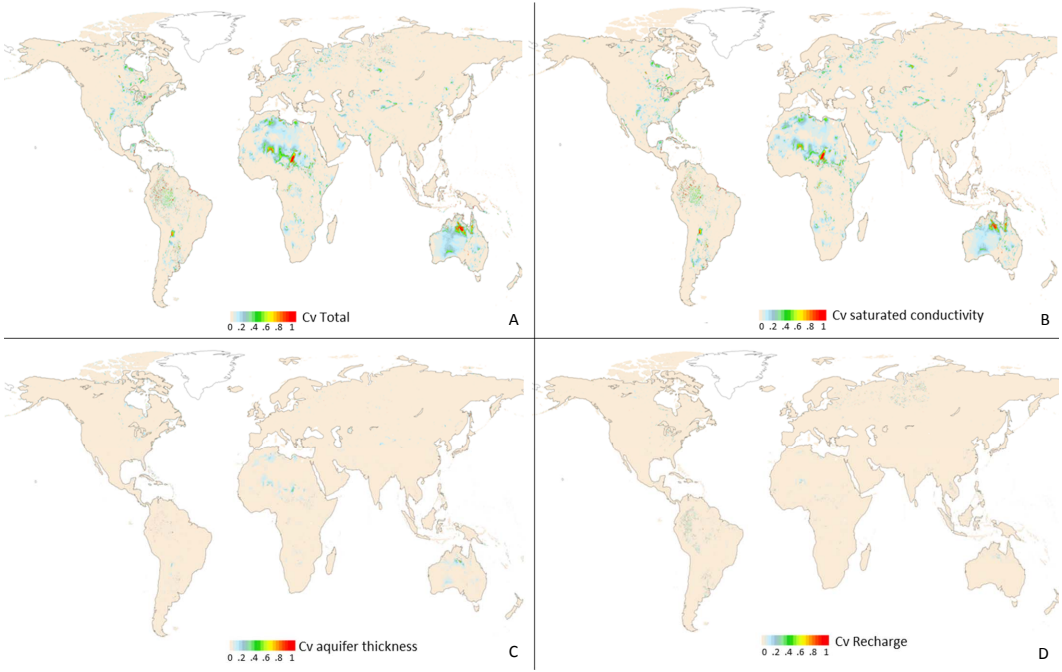

Figure 5. Coefficent of variation in groundwater depth: **(A)** of 1000 runs with different parameter settings for aquifer thickness, saturated conductivity, and groundwater recharge. **(B)–(D)** is the result of 100 runs with different parameter settings for one parameter.

HESSD
11, 5217–5250, 2014

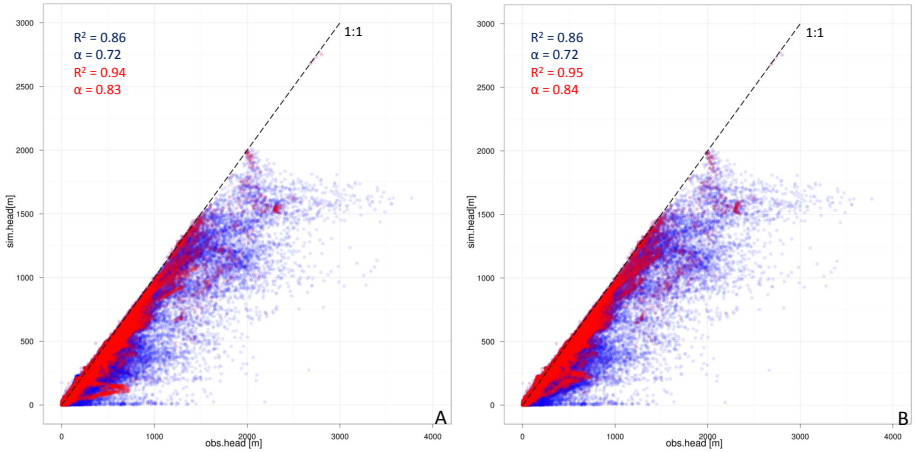

Figure 6. Scatter plots of observed heads against simulated heads for **(A)** best performing run and **(B)** best performing run, excluding observations for local and perched water tables.

HESSD
11, 5217–5250, 2014

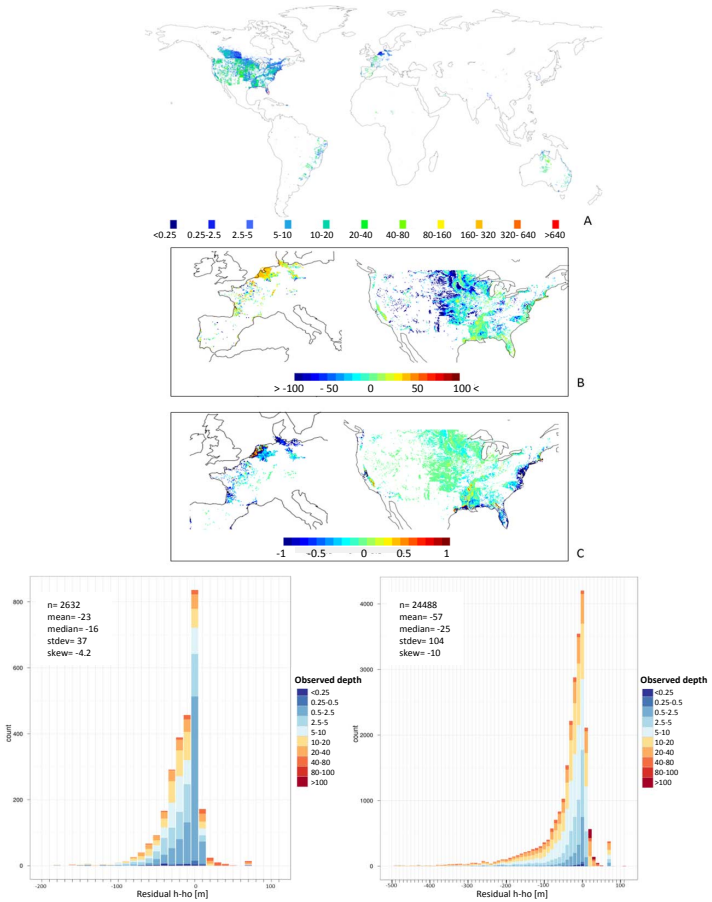

Figure 7. (A) Piezometer observations used for validation. **(B)** Maps of residuals (simulated head – observed head) for Europe and USA and **(C)** for relative residuals (residual/observed head). **(D)** Histograms of residuals for Europe and USA. Each bar in the histogram is clustered based on observed groundwater depth class.

HESSD
11, 5217–5250, 2014

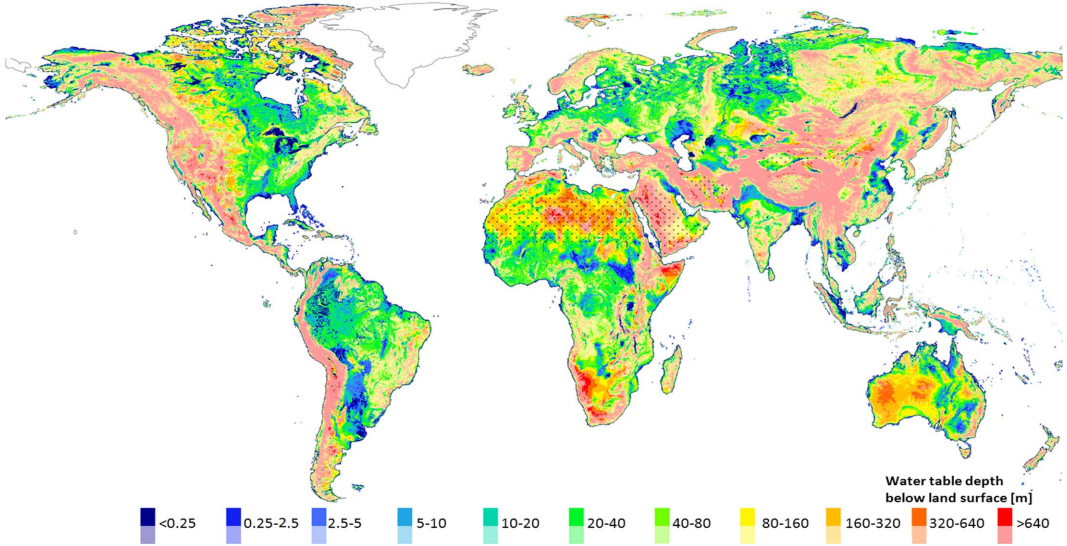

Figure 8. Simulated water table depth in meters below the land surface. The result of a steady-state natural run, using the best estimated parameter set. Whither colors indicate deep groundwater regions with most likely more shallow perched and local water tables not captured by the model. Dotted areas are hyper-arid zones.

HESSD
11, 5217–5250, 2014

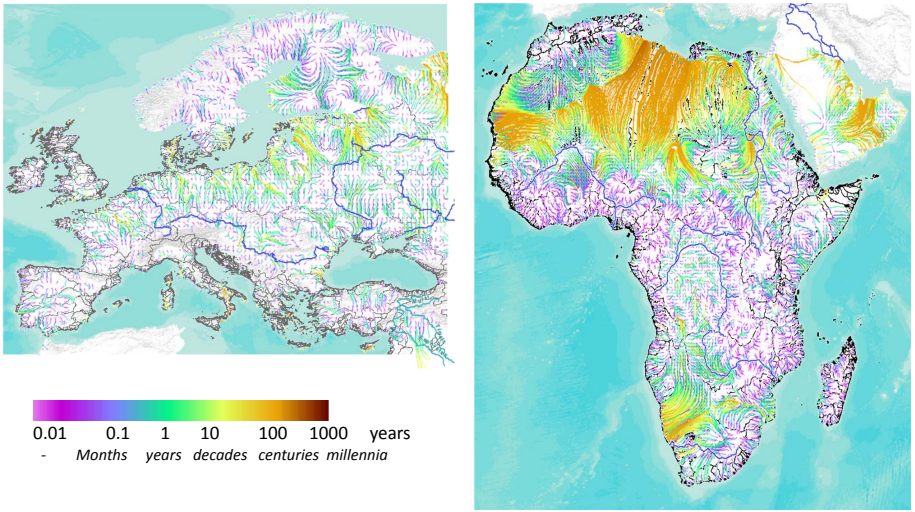

Figure 9. Flow paths simulated for (part of) Europe and Africa, underlain by river basin boundaries, overlain by major rivers.

HESSD
11, 5217–5250, 2014